

## WAVELET FRAME BASED COLOR IMAGE DEMOSAICING

JINGWEI LIANG

Department of Mathematics, Shanghai Jiao Tong University  
800 Dongchuan Road, Shanghai, China 200240

JIA LI

Department of Mathematics, National University of Singapore  
Block S17, 10 Lower Kent Ridge Road, Singapore 119076

ZUOWEI SHEN

Department of Mathematics, National University of Singapore  
Block S17, 10 Lower Kent Ridge Road, Singapore 119076

XIAOQUN ZHANG

Department of Mathematics and Institute of Natural Sciences, Shanghai Jiao Tong University  
800 Dongchuan Road, Shanghai, China 200240

(Communicated by the associate editor name)

**ABSTRACT.** Color image demosaicing consists in recovering full resolution color information from color-filter-array (CFA) samples with 66.7% amount of missing data. Most of the existing color demosaicing methods [13, 22, 14, 2, 23] are based on interpolation from inter-channel correlation and local geometry, which are not robust to highly saturated color images with small geometric features. In this paper, we introduce wavelet frame based methods by using a sparse wavelet [7, 19, 8, 20] approximation of individual color channels and color differences that recovers both geometric features and color information. The proposed models can be efficiently solved by Bregmanized operator splitting algorithm [24]. Numerical simulations of two data sets: McM and Kodak PhotoCD, show that our method outperforms other existing methods in terms of PSNR and visual quality.

**1. Introduction.** Most consumer-level digital cameras use single sensor (CCD/CMOS) to sample three color components like red, green and blue. Through color-filter-array (CFA) the sensor records one color per pixel location. In order to get a full-resolution color image, it is essential to interpolate the two missing color components. Since the CFA sample system has mosaic pattern for different colors, this process of recovering full-resolution images has been widely called as "color image demosaicing".

The most widely used CFA pattern is Bayer pattern [1] (see Figure 1). It measures green channel on a quincunx grid with subsampling rate 50% , and red and

---

2000 *Mathematics Subject Classification.* Primary:65T60, 68U10; Secondary: 94A08.

*Key words and phrases.* Wavelet frame, Color image restoration, demosaicing, denoising, inpainting.

J. Liang and X. Zhang were supported by the National Science Foundation of China (grant number: NSFC11101277 and NSFC11161130004) and by the Shanghai Pujiang Talent program(grant number 11PJ1405900).

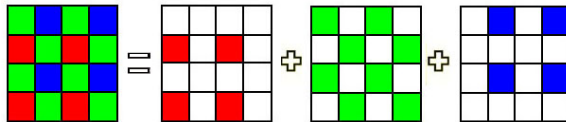


FIGURE 1. Bayer pattern used in single-chip digital cameras.

blue channels on rectangular grids with subsampling rate 25%, due to the fact that human eyes are generally more sensitive to green light.

Color image demosaicing can be essentially regarded as an image inpainting/interpolation problem. If we denote  $\Lambda_r$ ,  $\Lambda_g$  and  $\Lambda_b$  as the index sets for the observed red, green and blue pixels, respectively,  $\vec{f} = (f_r, f_g, f_b)^\top$  as the observed color vector and  $\vec{u} = (u_r, u_g, u_b)^\top$  as the unknown one, the observation model for color image demosaicing problem can be formulated as

$$\begin{cases} P_{\Lambda_r} u_r = f_r \\ P_{\Lambda_g} u_g = f_g \\ P_{\Lambda_b} u_b = f_b \end{cases} \quad (1)$$

where  $P$  is the usual projection operator. For simplicity, we rewrite the equation (1) in vector form as

$$P_\Lambda \vec{u} = \vec{f} \quad (2)$$

where  $P_\Lambda$  is the projection onto the tensor index sets  $\Lambda = \Lambda_r \times \Lambda_g \times \Lambda_b$ .

Recently, several wavelet frame based inpainting algorithms have been developed in literature (see [4, 5, 3, 9]) which shows clearly the advantage of the sparse wavelet frame approximation based method can reconstruct images better in terms of recovering edges and geometric features of images. This motivates us to explore the advantage of wavelet frame based method for color image demosaicing.

**1.1. Existing methods.** It is obvious that the problem (2) is an underdetermined inverse problem with many possible solutions. Based on the assumption of smoothness of images, it is possible to approximate the missing data from the measured data in spatial domain by interpolation. The well-known interpolation method Hamilton-Adams [14] scheme first interpolates the green channel by taking into account the second order derivatives of the red (blue) channel, and then recover the red and blue by interpolating the channel difference  $u_r - u_g$  and  $u_b - u_g$ . The interpolation is efficient for images with low color saturation and smooth chromatic gradient. Later on many advanced works are done to improve the accuracy of interpolation using more directional gradient information, such as [22, 15, 21]. Some later work such as self-similarity driven method [2] and local directional interpolation with nonlocal adaptive thresholding method [23] combine the local with nonlocal color relevance information to avoid color artifacts for those high saturated images.

Besides interpolation in spatial domain, reconstruction via frequency-domain approach is popular in the past years. One consideration of frequency-domain approach is the application of ad-hoc diamond-shape low-pass filter [11]. Yet as we know that using low-pass filter cannot accurately keep sharp edges and tiny features. In recent years, some researchers have proposed some methods combining both spatial and frequency reconstruction [13, 16]. For example, the alternating

projection method [13], is a combination of spatial domain interpolation and projection onto a constraint set in the wavelet domain. Another method based on local polynomial approximation [18] mainly attempts to optimize the coefficients of the polynomials, which is essentially a frequency-domain approach since higher order polynomial usually corresponds to higher frequency part.

**1.2. Our approach.** Most of the existing demosaicing methods are based on either spatial smoothness or high color correlation. They would fail to recover sharp edges and small scale feature due to low pass filtering effects. In addition, as observed in several work [2, 23], natural images often present abrupt color changes and relatively high saturation. It is hard to infer the missing color information only by local color correlation. Therefore, we aim to propose a regularization type model which can simultaneously recover sharp edges and small important structures in each color channel while maintaining the color consistency. More precisely, we apply a sparse reconstruction model both on color components and channel differences using tight frame systems [7, 19, 8] in two stages. The main advantage of wavelet frame based approaches is that piecewise smooth images can be sparsely approximated by properly designed wavelet frames, and hence, the  $\ell^1$ -norm regularization of frame coefficients can bring us sparse representations which are closed to real images. Tight frame systems have shown robust performance in a large variety of image restoration tasks, such as in [4, 5, 3, 9]. For this particular application, we design a two-stage model in order to recover gradually the fine features and color information.

As there are two sparsity priori models in image restorations: *analysis* based approach and *synthesis* based approach. It is a well known fact that *analysis* based approach is suitable for relative smooth images and *synthesis* based approach recovers features and edges better (see e.g. [10]). We provide an easy criterion to automatically choose one of the two approaches based on mean color saturation. Essentially, based on a crude initial guess, we determine which method should be applied according to the Mean Saturation (MS) level. In particular, for Kodak test data set, 21 out of 24 images have MS less than a given threshold, and *analysis* method outperforms *synthesis* one. For McM images, 15 out of 18 have MS greater than the threshold, and *synthesis* approach performs better. This coincides with the fact mentioned above, since it is known that images in Kodak test data set are relatively smooth, while McM images have more features and sharp edges. This also shows numerically that MS used in this paper is a simple and reasonable criterion in practice. As a result, our method can outperform the best available methods at 2.2 dB at most and 0.5db on average for the total 42 test images. Finally, although our proposed method is iterative, it is fast taking into account of the quality of reconstructed images, for example, the LDI-NAT method of [23] has the closest PSNR value to our method, it takes more than one hour to process a  $500 \times 500$  image, while ours takes much less than one minute at a personal computer. This paper is to introduce wavelet frame based method into the area of demosaicing and to show that it can be used to improve the quality of demosaicing. The computation time, which is not the emphasis here, can be even shorten, for example, by using other coding language (we use matlab for code in this paper) and with the further improvement of algorithm.

The rest of paper is organized as follows. Section 2 gives a brief introduction of tight frame based sparse recovery models. The main method and algorithms for color image demosaicing will be described in Section 3. Finally, numerical results

on two data sets: McM and Kodak, will be presented in Section 4 in comparison with other methods along with Conclusions in Section 5.

## 2. Tight frame based sparse recovery models.

**2.1. Sparse recovery models.** It is well known that piecewise smooth images can be sparsely approximated by wavelet tight frames which can be numerically computed by  $\ell^1$ -norm regularization of frame coefficients. For the simplicity, the tight frame transform can be written in matrix form, forward transform matrix  $W$  and inverse transform matrix  $W^T$ , the tight frame property implies that  $W^T W = I$ , while the identity  $W W^T = I$  does not necessarily hold. In computation, we do not use the matrix multiplication. Instead, we use the fast wavelet frame decomposition and reconstruction algorithms (see r.g., [8]), a brief introduction of wavelet tight frame will be given in subsection 2.2.

Next, we introduce two models: the *analysis* based approach and the *synthesis* based approach. The *analysis* based approach for tight frame demosaicing can be formulated as a constrained minimization problem

$$\min_{\vec{u}} |W\vec{u}|_1 \quad s.t. \quad P_{\Lambda}\vec{u} = \vec{f} \quad (3)$$

where  $|\cdot|_1$  means  $\ell^1$ -norm sum on each component. Meanwhile, the *synthesis* based approach solves the following problem

$$\min_{\vec{d}} |\vec{d}|_1 \quad s.t. \quad P_{\Lambda}W^T\vec{d} = \vec{f} \quad (4)$$

where  $\vec{d}$  is the coefficients of  $\vec{u}$  in the tight frame transform domain.

As pointed out before, the *analysis* based approach tends to recover smooth images with fewer artifacts, while the *synthesis* based approach tends to explore more sparsity in the transform domain, hence, it recovers features and sharp edges better. We might apply different models for different images.

**2.2. Wavelet tight frame.** We briefly introduce the concept of wavelet tight frame here. Interested readers can consult [20] for a short survey on theory and applications of frames, and [10] for a more detailed note.

A countable set  $X \subset L_2(\mathbb{R})$  is called a tight frame of  $L_2(\mathbb{R})$  if

$$f = \sum_{h \in X} \langle f, h \rangle h \quad \forall f \in L_2(\mathbb{R}), \quad (5)$$

where  $\langle \cdot, \cdot \rangle$  is the inner product of  $L_2(\mathbb{R})$ . Given a finite collection of functions  $\Psi = \{\psi_1, \psi_2, \dots, \psi_m\}$ , define  $X = \{\psi_{n,k,i} = 2^{n/2}\psi_i(2^n \cdot -k), 1 \leq i \leq m\}$ . If  $X$  is a tight frame, then  $X$  is called a wavelet tight frame and  $\Psi$  is called wavelet. The multi-resolution analysis (MRA) based wavelet can be generated by the unitary extension principle (UEP) of [19]. In particular, we use B-spline wavelet frame of orders (0, 1, and 3) constructed in [19]. For example, the 0th order of B-spline wavelet frame is a constant function and the corresponding wavelet tight frame is nothing but Haar wavelet frame [26], the other two are piecewise linear and cubic spline wavelet frame. Given a 1-D wavelet frame system for  $L_2(\mathbb{R})$ , the corresponding 2-D wavelet tight frame system for  $L_2(\mathbb{R}^s)$  can be constructed via the tensor products of 1-D wavelet frame (see e.g. [7, 10]).

The discrete wavelet transform can be generated by the filters of wavelets and corresponding refinable function that generate the MRA. A discrete image  $u$  is an 2-D array. We will use  $W$  to denote fast tensor product wavelet frame decomposition

operator and use  $W^\top$  to denote the fast reconstruction operator. Then by the UEP [19], we have  $W^\top W = I$ , i.e.  $u = W^\top W u$  for any image  $u$ . When the multiple level decomposition is used, we will further denote an  $L$ -level wavelet frame decomposition of  $u$  as  $Wu = \{W_{l,i,j}u : 1 \leq l \leq L, (i,j) \in I\}$ , where  $I$  denotes the index set of all frame bands. More details on discrete algorithms of wavelet frame transforms can be found in [10].

The wavelet frame system is a redundant system. The redundancy can reduce the amplification of possible error such as noise and artifacts generated during reconstruction process. More details on discrete algorithms and their relative analysis of wavelet frame transforms can be found in [10].

**3. A two-stage wavelet frame based method.** In this section, we propose a two-stage color image demosaicing method. First of all, as used in several existing demosaicing methods, color differences are used to interpolate unknown color channels since they are smoother than individual channel in most of natural images. Instead of applying regularization independently on each channel  $u_r, u_g, u_b$ , we first apply regularization on the green channel  $u_g$  and the inter-channel differences  $u_{rg} := u_r - u_g$  and  $u_{bg} := u_b - u_g$  to take advantage of color correlation. According to saturation degree, we apply automatically either sparsity-promoting *synthesis* based approach or smoothness-promoting *analysis* based approach. More precisely, *synthesis* based approach is applied to get highly sparse approximation for images with high saturation and abrupt color changes, and *analysis* based approach is more suitable for those having low saturation with smooth chromatic gradient. At the second stage, we apply a finer regularization on each channel  $u_r, u_g, u_b$  and the inter-channel differences  $u_{rg}, u_{gb} := u_g - u_b, u_{br} := u_b - u_r$  for correcting and recovering small structures while avoiding false colors. Here is the details the overall method:

1) **Stage 1.** For a given image, we apply one of either analysis based model or synthesis based model. Which one to use is according to the mean saturation value of an initial guess. The details on the criterion of choosing models by the mean saturation value of an initial guess will be given in Section 4.

Next, we describe the two specific models in details. For convenience, we redefine the vector  $\vec{u} = (u_{rg}, u_g, u_{bg})^T$  where  $u_{rg} = u_r - u_g$  and  $u_{bg} = u_b - u_g$ . Let  $\vec{\mu} = (\mu_{rg}, \mu_g, \mu_{bg})^T > 0$  be a regularization weight vector. The *analysis* based approach model is define as:

$$\begin{aligned} \min_{\vec{u}} \quad & \mu_{rg}|Wu_{rg}|_1 + \mu_g|Wu_g|_1 + \mu_{bg}|Wu_{bg}|_1 \\ \text{s.t.} \quad & \begin{cases} P_{\Lambda_r}(u_{rg} + u_g) = f_r; \\ P_{\Lambda_g}(u_g) = f_g; \\ P_{\Lambda_b}(u_g + u_{bg}) = f_b. \end{cases} \end{aligned} \quad (6)$$

Denote  $|W\vec{u}|_1 = (|Wu_{rg}|_1, |Wu_g|_1, |Wu_{bg}|_1)^T$ , then the above model can be rewritten as

$$\min_{\vec{u}} \quad \vec{\mu} \cdot |W\vec{u}|_1 \quad \text{s.t.} \quad A\vec{u} = \vec{f} \quad (7)$$

$$\text{where } A = \begin{bmatrix} P_{\Lambda_r} & P_{\Lambda_r} & 0 \\ 0 & P_{\Lambda_g} & 0 \\ 0 & P_{\Lambda_b} & P_{\Lambda_b} \end{bmatrix}.$$

Similarly we can define the *synthesis* based approach as

$$\min_{\vec{d}} \quad \vec{\mu} \cdot |\vec{d}|_1 \quad \text{s.t.} \quad AW^T\vec{d} = \vec{f} \quad (8)$$

where  $\vec{d} = (d_{rg}, d_g, d_{bg})^\top$  are the coefficients corresponding to  $u_{rg}, u_g, u_{bg}$ , respectively. The recovered color image is obtained by transforming the coefficients vector back to image space  $\vec{u} = W^\top \vec{d}$  and then sum up to get  $u_r, u_g, u_b$ . For both models, we observe that a low order wavelet filter gives a sufficient good result. The filter we used is Haar wavelet frame, for which 1-D filter is  $a_0 = \frac{1}{2}[1, 1], a_1 = \frac{1}{2}[1, -1]$ .

2) **Stage 2.** After the first stage, the image quality can be significantly improved, but we can still observe color artifacts. In order to refine small features and improve color consistence, we add more constraints and apply *synthesis* based approach on each color channel and the inter-channel differences. Let  $\vec{d} = (d_r, d_g, d_b, d_{rg}, d_{gb}, d_{br})^\top$  be the coefficients of  $u_r, u_g, u_b, u_{rg}, u_{gb}, u_{br}$  in tight frame transform domain respectively and  $\vec{\mu} = (\mu_r, \mu_g, \mu_b, \mu_{rg}, \mu_{gb}, \mu_{br})^\top$  be the weight parameter. We consider the following regularization model:

$$\min_{\vec{d}} \vec{\mu} \cdot |\vec{d}|_1 \quad s.t. \quad \begin{cases} P_{\Lambda_r} W^T(d_r) & = f_r; \\ P_{\Lambda_r} W^T(d_g + d_{rg}) & = f_r; \\ P_{\Lambda_r} W^T(d_b - d_{br}) & = f_r; \\ P_{\Lambda_g} W^T(d_r - d_{rg}) & = f_g; \\ P_{\Lambda_g} W^T(d_g) & = f_g; \\ P_{\Lambda_g} W^T(d_b + d_{gb}) & = f_g; \\ P_{\Lambda_b} W^T(d_r + d_{br}) & = f_b; \\ P_{\Lambda_b} W^T(d_g - d_{gb}) & = f_b; \\ P_{\Lambda_b} W^T(d_b) & = f_b. \end{cases} \quad (9)$$

Similarly, we can reformulate the above problem in a compact form as

$$\min_{\vec{d}} \vec{\mu} \cdot |\vec{d}|_1 \quad s.t. \quad BW^T \vec{d} = \vec{f} \quad (10)$$

$$\text{where } B = \begin{bmatrix} P_{\Lambda_r} & 0 & 0 & 0 & 0 & 0 \\ 0 & P_{\Lambda_r} & 0 & P_{\Lambda_r} & 0 & 0 \\ 0 & 0 & P_{\Lambda_r} & 0 & 0 & -P_{\Lambda_r} \\ P_{\Lambda_g} & 0 & 0 & -P_{\Lambda_g} & 0 & 0 \\ 0 & P_{\Lambda_g} & 0 & 0 & 0 & 0 \\ 0 & 0 & P_{\Lambda_g} & 0 & P_{\Lambda_g} & 0 \\ P_{\Lambda_b} & 0 & 0 & 0 & 0 & P_{\Lambda_b} \\ 0 & P_{\Lambda_b} & 0 & 0 & -P_{\Lambda_b} & 0 \\ 0 & 0 & P_{\Lambda_b} & 0 & 0 & 0 \end{bmatrix}. \quad \text{Note that we do not need}$$

to store the whole matrix of  $B$ , since the matrix vector multiplication and its adjoint can be easily implemented. In this step, in order to reconstruct finer structures, we apply piecewise linear wavelet frame  $a_0 = \frac{1}{4}[1, 2, 1], a_1 = \frac{1}{4}[-1, 2, -1], a_2 = \frac{\sqrt{2}}{4}[1, 0, -1]$ .

**3.1. Algorithms.** To implement these two steps, we need to solve the *synthesis* based approach (8) and (10), and *analysis* based approach (7). For the past few years, there developed a large amount of efficient algorithms for solving these two classes of problems arising in image processing and compressive sensing, such as Bregman based methods [17, 12] and other augmented Lagrangian based, splitting based methods. Among them, we will apply Bregman operator splitting algorithm (BOS) proposed in [24] since it can maximally decouple the variables when  $A^T A$  is not identity matrix. BOS is a method based on Bregman iteration and forward-backward operator splitting [6], which can transfer the constrained problem into

several easy and efficient subproblems without inner iterations. Another advantage of the algorithms is that it can be easily implemented in parallel which is attractive for large size image processing problems. BOS can be also interpreted as an inexact Uzawa method under the primal dual framework [25] and it can be applied in a large variety of inverse problems. For more applications and convergence proofs on this type of method, one can refer to [24, 25].

In the following, we will directly apply BOS method on both *synthesis* based and *analysis* based approaches. We take the *synthesis* based model (8) as an example. Starting from an initial guess  $\bar{u}^0$ , we set  $\bar{v}^0 = \bar{d}^0 = W\bar{u}^0, \bar{f}^0 = \bar{f}$ . Then for  $k = 0, \dots, K$ , we have

$$\begin{cases} \bar{v}^{k+1} &= \bar{d}^k - \delta W A^T (A W^T \bar{d}^k - \bar{f}^k) \\ \bar{d}^{k+1} &= \arg \min_{\bar{d}} (\bar{\mu} \cdot |\bar{d}|_1 + \frac{1}{2\delta} \|\bar{d} - \bar{v}^{k+1}\|^2) \\ \bar{f}^{k+1} &= \bar{f}^k + (\bar{f} - A W^T \bar{d}^{k+1}) \end{cases} \quad (11)$$

It is well known now that the second subproblem can be efficiently solved by the pointwise "shrinkage" operation:

$$\bar{d}^{k+1} = \text{shrinkage}(\bar{v}^{k+1}, \bar{\mu}\delta) := \text{sign}(\bar{v}^{k+1}) \max(|\bar{v}^{k+1}| - \bar{\mu}\delta, 0). \quad (12)$$

The problem (10) is solved in an analogous way by replacing the matrix  $A$  by  $B$  and the variables accordingly. For *analysis* based approach (7), we apply BOS method and obtain the following iteration scheme:

$$\begin{cases} \bar{v}^{k+1} = \bar{u}^k - \delta A^T (A \bar{u}^k - \bar{f}^k) \\ \bar{u}^{k+1} = \arg \min_{\bar{u}} (\frac{1}{2\delta} \|\bar{u} - \bar{v}^{k+1}\|^2 + \frac{\lambda}{2} \|W\bar{u} + \bar{b}^k - \bar{d}^k\|^2) \\ \bar{d}^{k+1} = \arg \min_{\bar{d}} (\bar{\mu} \cdot |\bar{d}|_1 + \frac{\lambda}{2\delta} \|\bar{d} - (W\bar{u}^{k+1} + \bar{b}^k)\|^2) \\ \bar{b}^{k+1} = \bar{b}^k + (W\bar{u}^{k+1} - \bar{d}^{k+1}) \\ \bar{f}^{k+1} = \bar{f}^k + (\bar{f} - A\bar{u}^{k+1}) \end{cases} \quad (13)$$

Since  $W^T W = I$ , the second subproblem has a close formula and the third one is also solved by the shrinkage formula (12).

**4. Numerical results.** In this section, we show the numerical results performed on the simulated mosaic images from two standard test data sets: McM dataset introduced in [23] and Kodak PhotoCD<sup>1</sup>. Due to space limit, only a subset of 8 images for each dataset is shown in Figure 2.

For the choice of parameters in our method, the two parameters  $\delta$  and  $\lambda$  in the algorithms (11) and (13) are fixed as 1 according to the convergence requirements of algorithms. Like self-similarity driven demosaicing [2], our initial guess  $\bar{u}^0$  is obtained by Hamilton-Adams scheme. In the first stage, the  $\ell^1$ -norm of the frame coefficients  $\|d_{r,g}^0\|_1, \|d_g^0\|_1, \|d_{b,g}^0\|_1$  are calculated to define the weight vector,  $\bar{\mu} := \mu_g (\frac{\|d_{r,g}^0\|_1}{\|d_g^0\|_1}, 1, \frac{\|d_{b,g}^0\|_1}{\|d_g^0\|_1})$  for balancing different components. Finally, there is only one free parameter  $\mu_g$  to be tuned. On the other side, we note that theoretically the choice of  $\mu_g$  does not affect the results since the models (7), (8) and (10) remain the same. Therefore the choice of parameters for our proposed method is rather easy and stable in practical use.

In the following, we explain how to choose between the two approaches in stage 1 based on the mean saturation value of  $\bar{u}^0 = (u_r^0, u_g^0, u_b^0)$ . At a given pixel  $\bar{u}_{i,j}^0$ ,

<sup>1</sup>The images are obtained from the link: <http://r0k.us/graphics/kodak/>.

we adopt the usual saturation definition:  $\frac{\max(u_r, u_g, u_b) - \min(u_r, u_g, u_b)}{\max(u_r, u_g, u_b)}|_{(i,j)}$ , then the average over all pixels is defined as the mean saturation (MS)  $s$ . Finally, given a threshold  $\tau$ , we apply *synthesis* based approach if  $s \geq \tau$ , otherwise *analysis* based. For Kodak image set, there are 21 out of 24 images with MS less than 0.4, while for McM set, 15 out of 18 images have MS greater than 0.4. Our numerical results have show that the *synthesis* approach performs better on McM while the analysis approach performs better on Kodak. This demonstrates that MS level provides a simple criterion for automatically determining the sparse recovery model in practice.

Moreover, we compare our method with six existing methods: Hamilton-Adams scheme (HA) [14], alternative projection method (AP) [13], directional linear minimum mean square error estimation method (DLMSEE) [22], local directional interpolation method with nonlocal adaptive thresholding (LDI-NAT) [23], local polynomial approximation method (LPA) [18], self-similarity demosaicing method (SSD) [2]. The codes are downloaded from the authors' websites and the default parameters are used for each method.

The numerical simulations show that our method (TFD) is the only one which performs well on both McM and Kodak data sets. The average PSNR values of all 42 images from both data sets is given in Table 1, which shows that our method noticeably outperforms all other methods in terms of PSNR value. It performs clearly better for the McM image set. In particular, the PSNR values of the 8 McM images in Figure 2 by all methods are summarized in Table 2. Our method is much better than other methods and the only one close to ours is the LDI-NAT method, but it is much slower and performs poorly for the Kodak images. The zoom-in results are given in Figure 3, 4 and 5. Figure 3 shows that only our method can reconstruct different color objects without artifacts. In Figure 4 and 5, our method is able to recover the fine details and sharp edges while the other methods present more or less artifacts along the boundaries. Finally, the PSNR values for the 8 Kodak images from Figure 2 are given in Table 3. The zoom-in results for image 3 from this data set are given in Figure 6. We can see that except TFD and LPA, the other methods present severe false color artifacts. We note that although LPA method has PSNR value higher than ours by 0.4 dB on average for Kodak images, it has much lower than ours (about 3 dB lower) for McM images.

Finally, in terms of computation time, our iterative methods are obviously slower than non-iterative method, but it is much faster than patch based LDI-NAT method proposed in [23], for a McM image with  $500 \times 500$  pixels, it takes our methods at most 40 seconds while more than 1 hour for LDI-NAT method on a laptop with 2Ghz dual-core intel CPU and 2GB memory. We point out the BOS algorithm can be further accelerated by either applying an adaptive parameters strategy or implementation in parallel, which can potentially reduce the computation time in real application. As we mentioned early that our focus here is to introduce the wavelet frame based method into color image demosaicing, since the wavelet frame based method has been proven efficient (see e.g. [10]).

TABLE 1. total average PSNR value (dB) of the demosaicing results for all 42 images of two datasets.

HA	DLMSEE	AP	SSD	LPA	LID-NAT	TFD
36.29	38.04	36.86	37.14	38.34	37.36	<b>38.90</b>





McM images



Kodak images

FIGURE 2. Subsets of images for MCM and Kodak image sets.

**5. Conclusions.** This paper presents wavelet tight frame based method for color image demosaicing problem. By applying regularization on both color channels and inter channel differences, we allow the reconstruction result smooth in the cartoon parts and sharp at the edges while keep color consistence. Based on the mean saturation of an initial guess, our proposed method can automatically choose the better approach out of *analysis* based approach (7) or *synthesis* based approach (8) for the first step. In the second step, by enforcing the constraints and increasing the order of the wavelet filter, we can furtherly improve the image quality. It is shown in the experiments that the proposed approaches did generally better than the existing approaches on two different kinds of test data sets. The proposed method potentially can be applied for demosaicing problems with the presence of noise due to the nature of regularization. In future, we will explore more color statistics and regularization terms to automatically recognize and protect more types of features so that the color image demosaicing method can be improved advancingly.

#### REFERENCES

- [1] B. E. Bayer. Color imaging array. *U.S. Patent*, 3971065, 1976.
- [2] A. Buades, B. Coll, J.-M. Morel, and C. Sbert. Self-similarity driven color demosaicking. *IEEE Transactions on Image Processing*, 18(6):1192–1202, 2009.

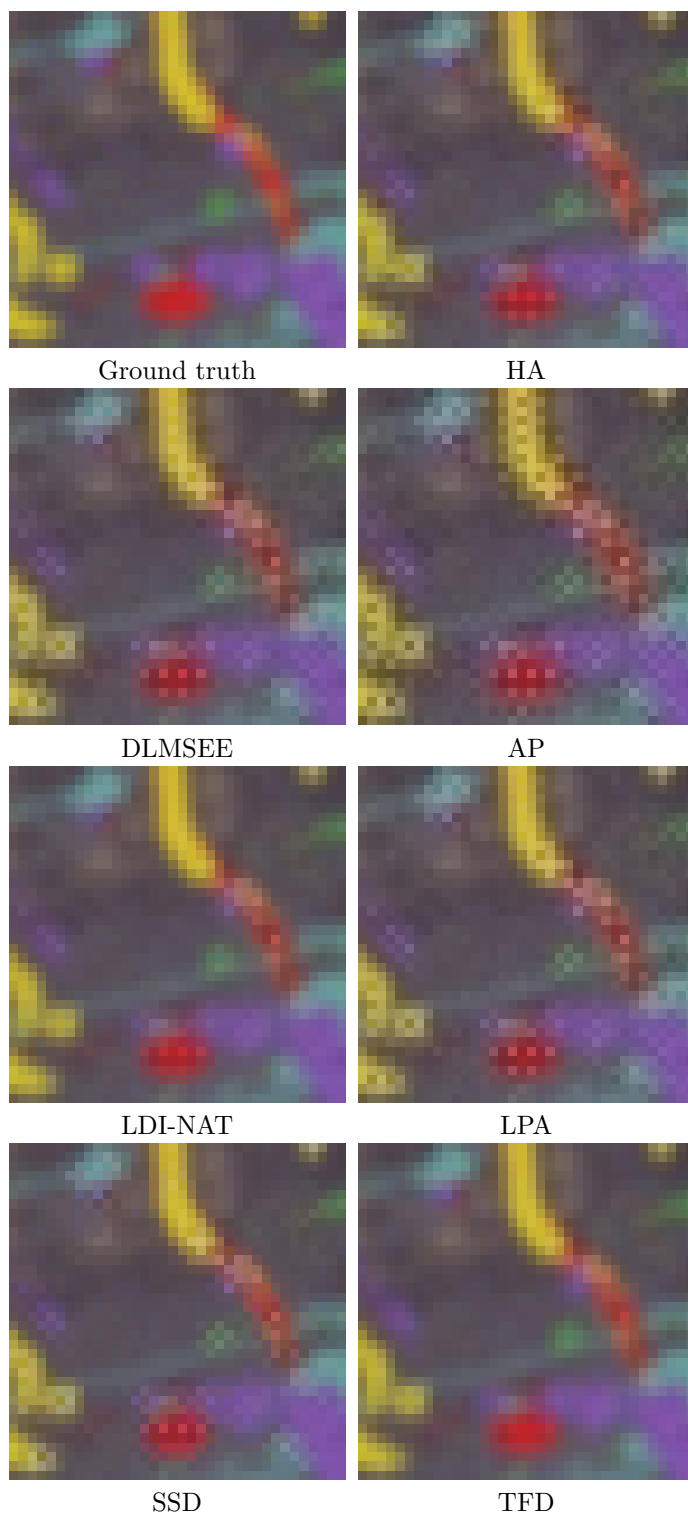


FIGURE 3. Zoom-in part of the demosaicing result for image 2 in MeM image set.

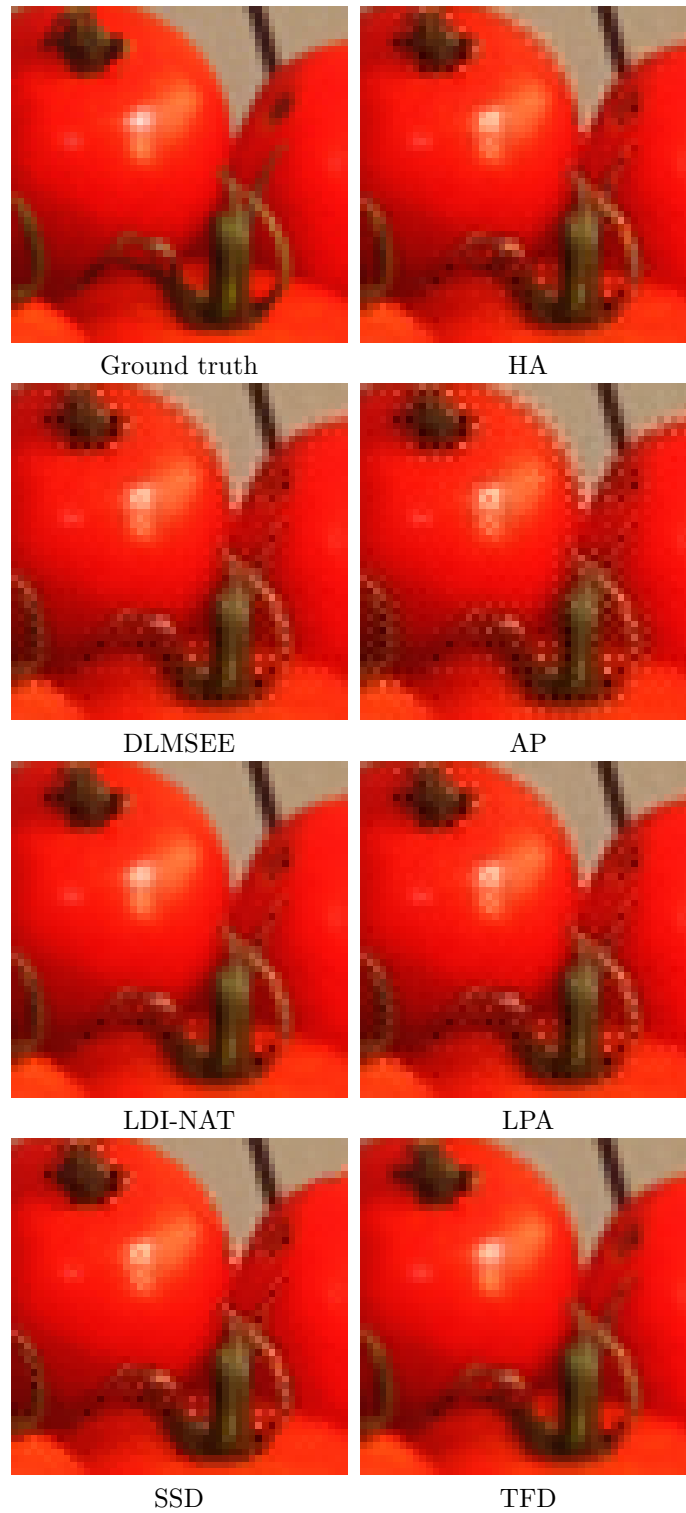


FIGURE 4. Zoom-in part of the demosaicing result for image 3 in MeM image set.

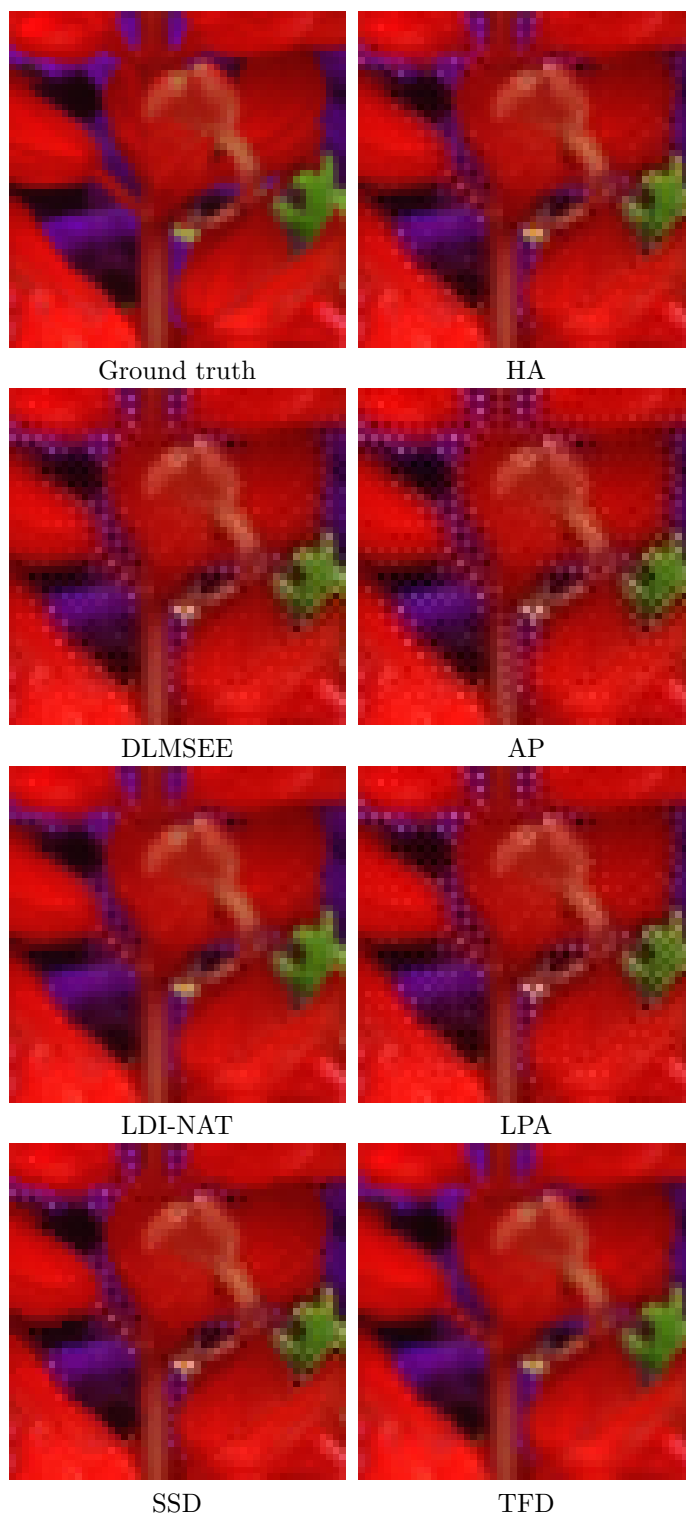


FIGURE 5. Zoom-in part of the demosaicing result for image 8 in MeM image set.

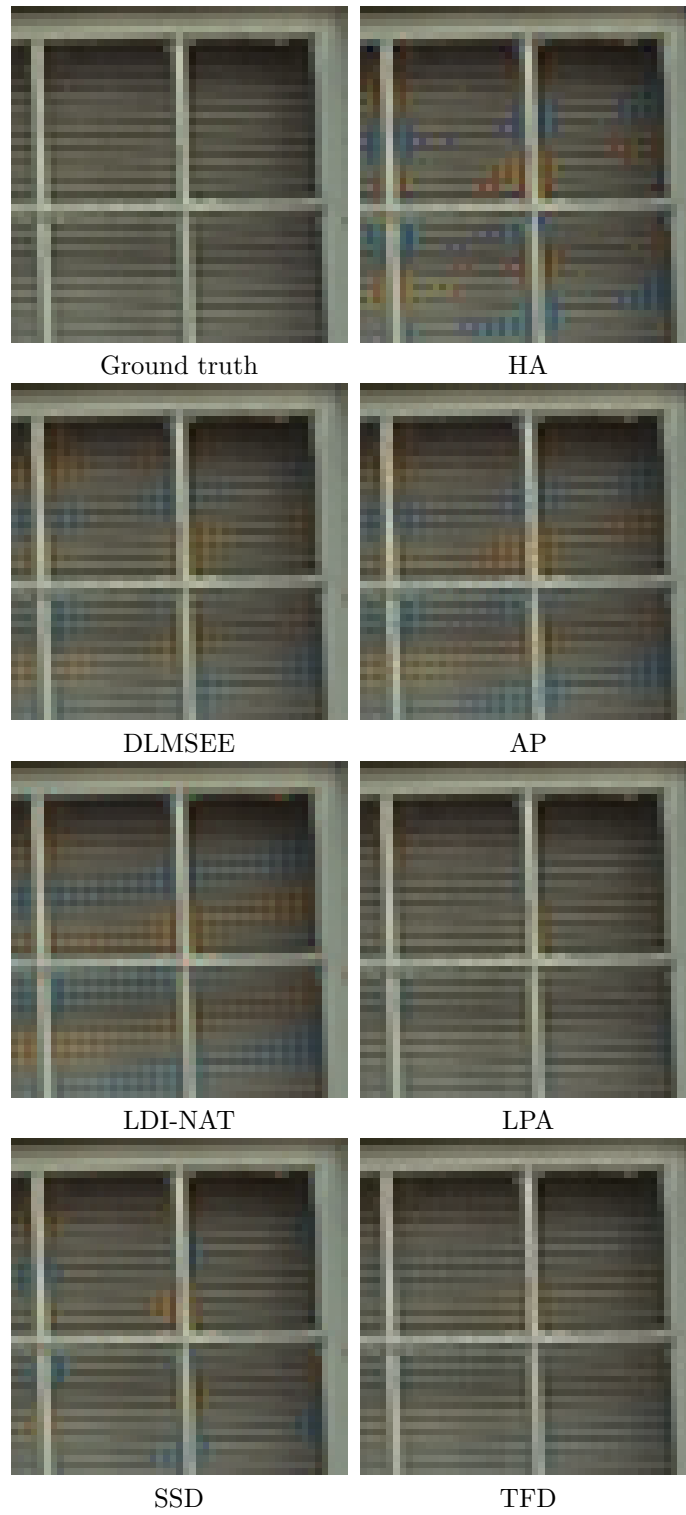


FIGURE 6. Zoom-in part of the demosaicing result for image 3 in Kodak image set.

Image		HA	DLMSEE	AP	SSD	LPA	LDI-NAT	TFD
1	R	33.79	33.30	32.08	33.85	33.51	<b>35.08</b>	34.77
	G	37.62	37.66	34.83	37.96	37.56	39.09	<b>39.15</b>
	B	32.21	31.86	31.18	32.24	32.06	<b>32.93</b>	32.80
2	R	36.60	34.98	32.80	36.89	35.30	39.36	<b>39.92</b>
	G	40.30	38.61	33.78	39.47	38.20	43.35	<b>44.42</b>
	B	32.95	31.15	30.30	32.72	31.94	34.96	<b>35.77</b>
3	R	34.01	32.39	31.68	34.45	33.31	35.50	<b>35.74</b>
	G	39.62	38.73	35.57	39.91	39.16	41.99	<b>42.14</b>
	B	35.55	34.66	33.80	35.92	35.10	36.43	<b>36.50</b>
4	R	36.19	34.70	33.89	36.82	35.69	<b>38.32</b>	37.95
	G	40.86	40.00	36.41	40.63	40.33	42.70	<b>42.77</b>
	B	36.25	35.55	34.57	36.50	35.99	36.87	<b>36.94</b>
5	R	37.72	36.91	35.65	38.46	37.72	<b>39.79</b>	39.39
	G	40.78	40.44	37.15	40.50	40.48	42.53	<b>42.61</b>
	B	36.52	35.75	35.40	37.27	36.14	<b>37.88</b>	37.59
6	R	36.06	35.32	34.79	36.50	35.82	37.01	<b>37.12</b>
	G	41.20	40.71	38.30	41.17	40.85	42.65	<b>42.92</b>
	B	37.98	37.30	36.58	38.32	37.60	38.98	<b>39.03</b>
7	R	32.58	31.95	29.76	32.58	30.64	<b>34.97</b>	34.76
	G	34.09	33.22	30.00	33.23	31.59	<b>35.59</b>	35.54
	B	29.57	28.06	27.79	28.87	27.51	32.16	<b>32.61</b>
8	R	29.99	28.32	27.39	29.90	28.54	32.13	<b>32.95</b>
	G	35.17	33.31	29.31	34.08	32.26	37.72	<b>38.47</b>
	B	29.31	27.77	27.20	29.06	27.82	30.98	<b>32.04</b>
Average		35.705	34.694	32.926	35.721	34.897	37.457	<b>37.663</b>

TABLE 2. PSNR value (dB) of the demosaicing results for 8 McM images in Figure 2.

- [3] J. Cai, R. Chan, L. Shen, and Z. Shen. Simultaneously inpainting in image and transformed domains. *Numerische Mathematik*, 112(4):509–533, 2009.
- [4] J.F. Cai, R.H. Chan, and Z. Shen. A framelet-based image inpainting algorithm. *Applied and Computational Harmonic Analysis*, 24(2):131–149, 2008.
- [5] J.F. Cai, R.H. Chan, and Z. Shen. Simultaneous cartoon and texture inpainting. *Inverse Problems and Imaging*, 4(3):379–395, 2010.
- [6] P. L. Combettes and V. R. Wajs. Signal recovery by proximal forward-backward splitting. *Multiscale Model. Simul.*, 4:1168–1200, 2005.
- [7] I. Daubechies. Ten lectures on wavelets. CBMS-NSF Lecture Notes, SIAM, nr. 61, 1992.
- [8] I. Daubechies, B. Han, A. Ron, and Z. Shen. Framelets: MRA-based constructions of wavelet frames. *Applied and Computational Harmonic Analysis*, 14(1):1–46, Jan 2003.
- [9] B. Dong, H. Ji, J. Li, Z. Shen, and Y. Xu. Wavelet frame based blind image inpainting. *Applied and Computational Harmonic Analysis*, to appear, 2011.
- [10] B. Dong and Z. Shen. MRA based wavelet frames and applications. *IAS Lecture Notes Series, Summer Program on "The Mathematics of Image Processing"*, Park City Mathematics Institute, 2010.
- [11] J. W. Glotzbach, R. W. Schafer, and K. Illgner. A method of color fillter array interpolation with alias cancellation properties. *IEEE Int. Conf. Image Processing*, 1:141–144, 2001.
- [12] T. Goldstein and S. Osher. The split Bregman algorithm for L1 regularized problems. *SIAM Journal on Imaging Sciences*, 2(2):323–343, 2009.
- [13] B. Gunturk, Y. Altunbasak, and R. M. Mersereau. Color plane interpolation using alternating projections. *IEEE Transactions on Image Processing*, 11(9):997–1013, 2002.

Image		HA	DLMSEE	AP	SSD	LPA	LDI-NAT	TFD
1	R	40.54	41.78	41.28	40.73	<b>42.52</b>	40.76	42.33
	G	42.06	45.24	43.85	43.05	45.38	43.39	<b>45.54</b>
	B	40.16	41.00	40.75	41.00	<b>41.73</b>	40.51	41.70
2	R	39.70	42.49	41.24	40.61	<b>42.85</b>	39.80	42.64
	G	41.29	45.31	43.84	42.33	45.54	42.26	<b>45.59</b>
	B	39.25	41.23	40.77	40.64	<b>41.79</b>	39.39	41.53
3	R	33.11	37.53	36.53	34.65	<b>39.43</b>	33.58	38.85
	G	34.58	40.17	40.32	36.21	<b>42.43</b>	35.64	42.03
	B	33.22	37.96	37.05	36.12	<b>39.87</b>	33.95	39.66
4	R	37.98	43.53	40.92	39.55	<b>43.65</b>	38.25	43.34
	G	39.42	45.68	44.63	40.92	45.97	40.52	<b>46.34</b>
	B	37.76	42.42	40.63	40.30	<b>42.59</b>	38.13	41.91
5	R	36.74	40.34	38.29	37.90	<b>40.80</b>	36.67	39.69
	G	38.29	42.91	42.38	39.52	43.47	39.05	<b>43.50</b>
	B	36.78	40.07	39.05	38.66	<b>40.53</b>	36.69	40.03
6	R	38.74	41.77	40.75	39.99	<b>41.84</b>	39.44	41.43
	G	39.80	43.85	43.42	41.33	43.96	41.20	<b>44.45</b>
	B	37.27	39.23	38.93	38.64	<b>39.55</b>	38.03	39.13
7	R	34.97	39.07	38.14	36.49	39.58	35.35	<b>39.76</b>
	G	36.22	41.15	41.46	37.95	41.87	37.27	<b>42.63</b>
	B	34.40	37.58	37.35	36.38	<b>37.94</b>	34.98	37.84
8	R	35.69	37.51	36.99	36.06	<b>37.52</b>	36.55	36.70
	G	37.60	40.78	39.59	38.15	40.72	38.76	<b>40.92</b>
	B	35.49	37.35	36.62	36.42	<b>37.46</b>	36.32	37.42
Average		37.543	41.080	40.199	38.900	<b>41.625</b>	38.188	41.264

TABLE 3. PSNR value (dB) of the demosaicing results for 8 Kodak images in Figure 2.

- [14] J. Hamilton Jr and J. Adams Jr. Adaptive color plan interpolation in single sensor color electronic camera. *U.S. Patent*, 5:629–734, 1997.
- [15] R. Kakarala and Z. Baharav. Adaptive demosaicing with the principal vector method. *IEEE Transactions on Consumer Electronics*, 48(4):932–937, 2002.
- [16] W. Lu and Y.P. Tan. Color filter array demosaicking: New method and performance measures. *IEEE Transactions on Image Processing*, 12(10):1194–1210, 2003.
- [17] S. Osher, M. Burger, D. Goldfarb, J. Xu, and W. Yin. An iterative regularization method for total variation-based image restoration. *Multiscale Model. Simul.*, page 460C489, 2005.
- [18] D. Paliy, V. Katkovnik, R. Bilcu, S. Alenius, and K. Egiazarian. Spatially adaptive color filter array interpolation for noiseless and noisy data. *International Journal of Imaging Systems and Technology*, 17(3):105–122, 2007.
- [19] A. Ron and Z. Shen. Affine systems in  $l_2(\mathbb{R}^d)$ : The analysis of the analysis operator. *Journal of Functional Analysis*, 148(2):408–447, 1997.
- [20] Z. Shen. Wavelet frames and image restorations. *Proceedings of the International Congress of Mathematicians, Hyderabad, India*, 2010.
- [21] C.-Y. Tsai and K.-Tai Song. Heterogeneity-projection hard-decision color interpolation using spectral-spatial correlation. *IEEE Transactions on Image Processing*, 16(1):78–97, 2007.
- [22] L. Zhang and X. Wu. Color demosaicking via directional linear minimum mean square-error estimation. *IEEE Transactions on Image Processing*, 14(12):2167C2178, 2005.
- [23] L. Zhang, X. Wu, A. Buades, and X. Li. Color demosaicking by local directional interpolation and non-local adaptive thresholding. *Journal of Electronic Imaging*, 20(2):023016, 2011.

- [24] X. Zhang, M. Burger, X. Bresson., and S. Osher. Bregmanized nonlocal regularization for deconvolution and sparse reconstruction. *SIAM Journal on Imaging Sciences*, 3(3):253–276, 2010.
- [25] X. Zhang, M. Burger, and S. Osher. A unified primal-dual algorithm framework based on bregman iteration. *Journal of Scientific Computing*, 46(1):20–46, 2010.
- [26] Haar A. Zur. Theorie der orthogonalen funktionensysteme. *Mathematische Annalen*, 69:331–371, 1910.

Received July 2012.

*E-mail address:* Jingwei Liang jingwei.leung@gmail.com

*E-mail address:* Li Jia lijia@nus.edu.sg

*E-mail address:* Shen Zuwei matzuows@nus.edu.sg

*E-mail address:* Xiaoqun Zhang xqzhang@sjtu.edu.cn